Article

Increasing Structural Performance of Space Telescope Mirrors through Simultaneous Shape and Size Optimization

Marcel Warzecha [1,†], Markus E. Schatz [2,*,†,‡] , Stefano Lucarelli [3,†] and Cedric Jüttner [4,†]

1 TU Munich, 80333 München, Germany
2 DHBW Ravensburg, 70174 Stuttgart, Germany
3 AIRBUS Defence & Space GmbH, 82024 Taufkirchen, Germany
4 Altair Engineering GmbH, Calwer Str. 7, 71034 Böblingen, Germany
* Correspondence: schatz.m@dhbw-ravensburg.de; Tel.: +49-176-53409900
† These authors contributed equally to this work.
‡ Current address: DHBW RV, Campus FN, Fallenbrunnen 2, 88045 Friedrichshafen, Germany.

Abstract: In this paper, a numeric optimization approach for designing space telescope mirrors will be presented. It is fundamental to space telescopes that each element—including their mirrors—are as lightweight as possible. Moreover, the performance of space telescopes is driven by how strongly these mirrors are distorted upon removal of gravitational load. These distortions result in a deterioration in the optical performance, which is also known as the wavefront error. This error can best be described via Zernike polynomials. To increase the optical performance, along with making the mirror lightweight, the overall root mean square (RMS) of the deformation is used as the optimization objective. An approach utilizing size and shape variables is used to define the feasible design space for the optimization. Lastly, general findings will be discussed, as well as numerical advantages of deploying structural optimization (e.g., robustness evaluation).

Keywords: telescope mirrors; structural optimization; size and shape design variables; wavefront error; gravity release; Zernike polynomials

1. Introduction

One day after Christmas Eve, the James Webb Space Telescope caught the world's attention; its launch marks a key milestone. This holds not only for space enthusiasts, but also for humanity, as it will serve as a successor to the well-known Hubble telescope. When it comes to designing such telescopes, the design of the primary mirror is of high importance, as it defines the telescope's light-gathering power and thus performance. Aside from the mere size, it is evident that its surface quality in space matters most. Knowing this, manufacturing such a mirror on earth requires engineers to make mirrors that are lightweight to the greatest possible extent, while still stiffening the underlying mirror support structure, such that it sustains the loads experienced during manufacturing, launch, and in service.

To thin out a mirror in an optimal fashion, the mirror's deformations upon removal of gravitational loads ought to be predicted as accurately as possible. For this purpose, finite element analysis (FEA) is utilized. In order to leverage FEA, the underlying finite element model (FEM) is parameterized and then optimized by use of numerical optimization algorithms. There is a multitude of papers emphasizing the success of design optimization of mirror structures [1]. For instance, Eberle (2006) optimized a rib-stiffened optical mirror, which is adaptive by means of piezo actuators. The FEM was discretized with hexahedral elements, and parameterization of the optimization model included rib thickness, positions, and size of piezo patches. These parameters were then considered as design variables [2] during numerical optimization runs. By doing so, the performance of the mirror has been improved considerably, as outlined by U.C. Müller [3]. Liu et al. realized a topology

optimization of a lightweight primary mirror designed to be used within a large-aperture space telescope in their work [4]. An optimized design was given by a lightweight support structure formed by a honeycomb pattern and tree-like stiffeners. An increase in performance by a tremendous 62.5% was achieved [4]. S. Lucarelli investigated many optical systems where, in demanding scenarios, optimization is a profound choice [5]. There are more relevant research works as well, highlighting the benefits of topology optimization of large-apearature space mirrors, such as the one performed by Qu et al. in 2018 [6].

Topology optimization may be regarded as a key technology for identifying lightweight structures with ease. However, as highlighted by one of the most renowned scientists in the field of topology optimization, Ole Sigmund, it may tend to local solutions, since filtering and stabilization does not allow resolving either shell or membrane structures [7] with commercial FEMs. For this reason, it has been decided to combine size and shape optimization with each other. This combination was realized by further introducing contact definitions to the FEM. This feature allowed morphing of ribs, in such a fashion that they slide past each other while still being properly connected in their intersection lines. Hence, with this research work, it will be shown how the combination of size and shape optimization are enriched via modern contact realization, thereby allowing one to achieve full freedom in designing mirror support structures. This approach was highlighted and discussed in [8], where the combination of gradient-based size and shape optimization yielded an optimal propeller design. It was key to this research work that each mating of ribs was abstracted utilizing *Altair*'s *HyperMesh*'s latest features in terms of general contact definition. These features ultimately yielded technically meaningful results.

2. Problem Description and Abstraction

Prior to an optimization, it is crucial to understand the underlying nature of the problem and abstract its physics, so that algorithms are capable of adjusting each parameter in an optimal fashion. Consequently, mirror deformations, as the key performance metric, and their assessment will be discussed next. Following this, the FE model, its parametrization, and the optimization problem are portrayed.

2.1. Mirror Deformation

It is essential to capture optical performance under mechanical loading so as to judge where to thicken or thin out a given space telescope mirror. Obviously, relevant mechanical loads originate from the removal of the gravitational load, as mirrors are manufactured on earth—clearly subjected to gravity load in different directions—and later operate in almost gravity-free space.

Rigid mirror deflections (and thus sole tilt) and the translation of mirror surfaces are not of relevance in the design of mirror structures, as these deflections are, in most cases, compensated with ease. For this reason, the relative displacement of mirror surfaces is of interest. Relative correlates to the distortion of the mirror surface after removal of the overall tilt and translation (i.e., the distortion without the rigid mirror deflection).

This is depicted in Figure 1, where the black line highlights a distorted mirror surface. The horizontal line refers to a mirror surface on earth (i.e., with gravity load), whereas the tilted blue line shows the translated and tilted surface of an undeformed mirror. Here, it shall be noted that the rigid mirror deformation may be regarded as a fit yielding minimum surface error. Therefore, these rigid modes may be understood as correction modes in terms of tilting and translation of the whole mirror.

To quantify surface quality or deviations from optimal surfaces (e.g., the blue line in Figure 1), the well-known Zernike polynomials [9] are most frequently used. These approximate the distorted surface by use of polynomials and hence indicate the resulting wavefront error (WFE).
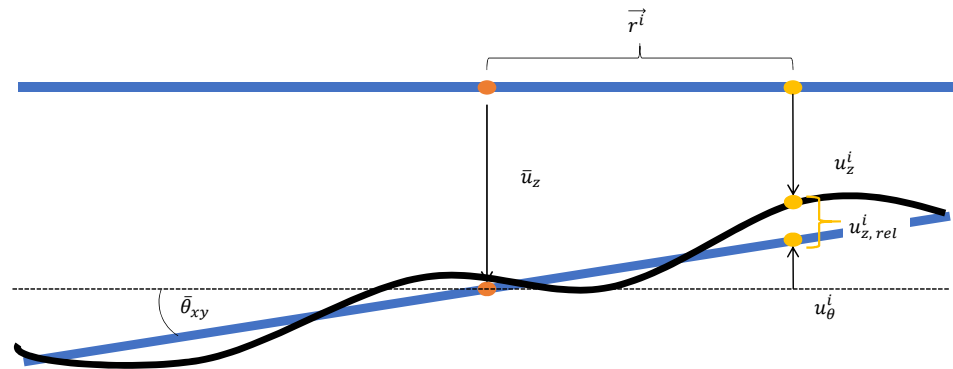
Figure 1. Deformation of mirror calculated from displacement.

As speed is, at least to some extend, crucial during optimizations, the full set of Zernike polynomials is solely evaluated at the end of each optimization run. During the iterations, the nature of describing the deviation from the ideal surface is considered as objective. This branch is followed, as this results in a tremendous speed-up, while no effect on the quality of search direction has been observed. For this reason, the following equation was considered as objective, where the overall distortion was gathered via the *RMS* of relative displacements (see Figure 1 above):

$$RMS(\vec{u}^i_{z,rel}) = \sqrt{\frac{1}{n}\sum_{i=1}^{n}\vec{u}^i_{z,rel}{}^2} \tag{1}$$

As given, Equation (1) provides the root mean square (RMS) based on relative mirror deflection in z direction (i.e., $u^i_{z,rel}$). In practice, this equation is evaluated by computing the relative displacement for each node $i \in [1, n]$, as follows in Equation (2):

$$\vec{u}^i_{rel} = \vec{u}^i - \overline{\overline{u}} - \overline{\overline{\theta}} \times \vec{r}^i, \tag{2}$$

where $\vec{u}^i$, $\overline{\overline{u}}$ and $\vec{r}^i$ represent the displacement vector of node i, rigid mirror displacement at center, and geometric lever of node i (distance mirror center to node i), respectively. $\overline{\overline{\theta}}$ describes the tilt of the rigid mirror displacement and is needed to yield the relative displacement (see yellow bracket in Figure 1).

As a side remark, one could realize a certain speed-up in the case that one does not loop over all nodes, but instead considers each third node, reducing the amount of equations, such as in (2), down to one-third. By doing so, one should ensure that the pattern of the considered nodes is asymmetric, while still covering the whole mirror. This reduction is not realized next, but it is proven to work very well.

2.2. Finite Element Model

One of the relevant, if not the most relevant, aspect of abstracting the problem is the finite element model (FEM). This particularly holds in the case where numerical optimization is deployed, as the FEM literally guides the algorithm where to thin out. Consequently, by abstracting a mirror towards an FEM, all relevant modes of deflection shall be reflected with high quality. Following this, it has been decided to use *Altair*'s *HyperMesh* for two reasons. First and foremost, it is the baseline tool for meshing and FEM generation within *AIRBUS Defence and Space GmbH*. Secondly, it allows one to define design variables with ease. This aspect is addressed separately in Section 2.4.

In Figure 2, the FEM is depicted, where Figure 2a portrays the support on the outer support ring of the space mirror and Figure 2b on the inner, respectively. However, the rest of the FEM remains the same. Both boundary conditions have been set up such that radial extension does not result in stresses and are therefore not tied. In that sense, all other degrees of freedom—except the radial elongation—are pinned.
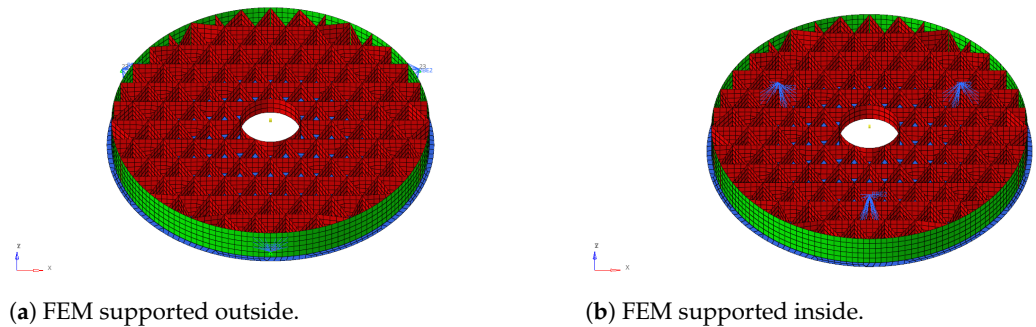
(**a**) FEM supported outside.   (**b**) FEM supported inside.

Figure 2. Finite element models with two different support cases.

In practice, this boundary condition is realized through support blades addressing thermo-elastic deflections. The FEM is discretized using *Altair*'s *HyperMesh* with 9500 nodes and 10,500 shell elements. For ensuring sufficient accuracy, a convergence study on deflections has been realized. The dimensions of the mirror are 1 m in diameter and 10 cm for the initial height. By the subsequent optimization loops, the height has been increased up to 20 cm. Aluminum was chosen to be the material the mirror is made of. The material assigned to the FEM has basically no impact on the quality of the optimization results; however, it does determine certain boundary conditions (e.g., the minimum thickness of ribs, which is driven by manufacturing capabilities).

At this point in time, it shall be highlighted that mechanical stresses are not of relevance here. The reasoning is threefold: First, large-scale space telescope mirror design is primarily driven by mass and stiffness distribution [10]. Second, minimizing wavefront error reduces the overall weight of the space telescope mirrors. The light weight, as a consequence, alleviates high loading, as the mirror is loaded via gravitational forces. Last but not least, local stress overshoots are often addressed by local design features such as slight thickening, or by introducing curvatures or chamfers.

The baseline design of this study was realized with a light-weighting factor of 90 and aluminum as the baseline material. For obvious reasons, material or overall size might be scaled. However, the approach and subsequent findings remain valid to almost the full extent.

2.3. Pattern Identification

It is crucial to space telescope mirror design to not only find an optimum, but also to understand how its derived design features imprint on the actual mirror's deflections. The following principles shall be adhered to in order to make a given design plausible. Thus, before going into local design refinement or even manufacturing, the underlying physics in terms of load paths and stiffening structures shall be deliberately studied. In addition, one ensures that artificial optima caused by modeling imperfections and the like are excluded.

For realizing the above-mentioned principle, a sequence of trades has been performed prior to actual optimization runs. These trades aimed at identifying patterns. Patterns are thereby formed by either identifying components warping in tandem or displaying similar levels of strain energy under loading. In order to do so, evaluation of element strain energy density, as a conflation of mechanical load and deformation, serves best to find these patterns. This holds, as neither stress nor strain alone would allow one to identify load transmission paths with certainty; it is the combination of both that determines load paths.

In Figure 3, the developed process of optimizing space mirrors is depicted. As given there, the modeling and definition of the design space marks the beginning. Note that the design space is given by the set of design variables, comprising size and shape variables. Herein, the design space is formed by the thicknesses of each rib section, the ring, and the mirror surface itself, as well as the shape and contour of the ribs. For identifying sections, an initial FEA is conducted, based on which the element strain energy densities (ESE) are evaluated. These ESE are acquired for either identifying or refining existing patterns. If no additional pattern is to be identified, the optimization is launched. Optimization software *OptiStruct* has been chosen, as its algorithms are based on analytic sensitivities, making it precise and efficient. In addition, *OptiStruct* allows one to incorporate various system responses off the shelf, as well as user-defined responses, which can be designed using Altair Compose and its open matrix language (OML).
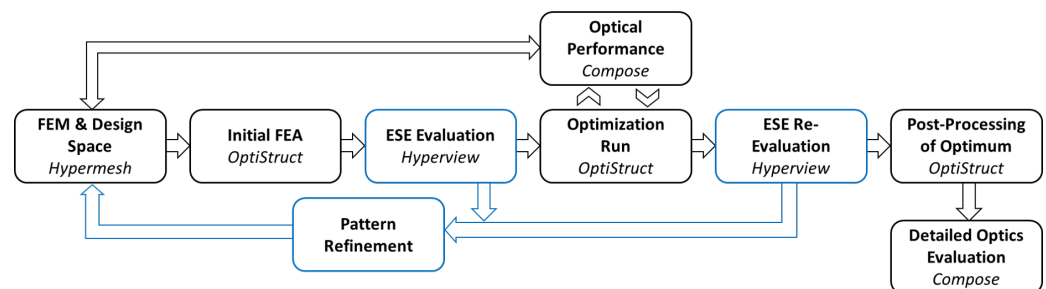

Figure 3. Optimization process where iterative pattern refinement is highlighted in blue.

Once the optimization is converged, the patterns and their technical (and therefore mechanical) behavior is re-checked. In case no refinement is necessary, the actual post-processing is realized. It is relevant to note that *OptiStruct*, being gradient-based, allows the interpretation of optima by studying sensitivities without additional efforts. This, for instance, allows the interpretation of robustness via a linearization at a given optimum. The reader shall note that more details regarding this are given in Section 4.2.

2.4. Actual Model Parameterization

This sections aims at highlighting the key geometric patterns as identified based on ESE evaluation (see Section 2.3). These patterns are discussed next. The depicted patterns yield homogeneous ESE distributions when all parameters, such as thickness, rib height, and rib position, are chosen in an optimal fashion.

As can be observed in Figure 4, there are two main rib types (#1 Figure 4a and #2 Figure 4c). These were labeled as main, as they both provide global stiffness, suppressing bending and torsion of the respective mirror axis. Another key geometric feature is given by Figure 4e, namely the inner and outer ring. They are both regarded as crucial, as they steer global twisting, torsion, and bending of the mirror surface. Figure 4b,d both depict minor rib patterns, which have a strong impact on local mirror surface deformations such as wrinkling.

Aside from the above-mentioned dominant patterns, one might identify more. However, our parameter studies revealed that further decomposition yields patterns of subordinate relevance. For this reason, the patterns as discussed serve as the basis for all subsequent optimization results.
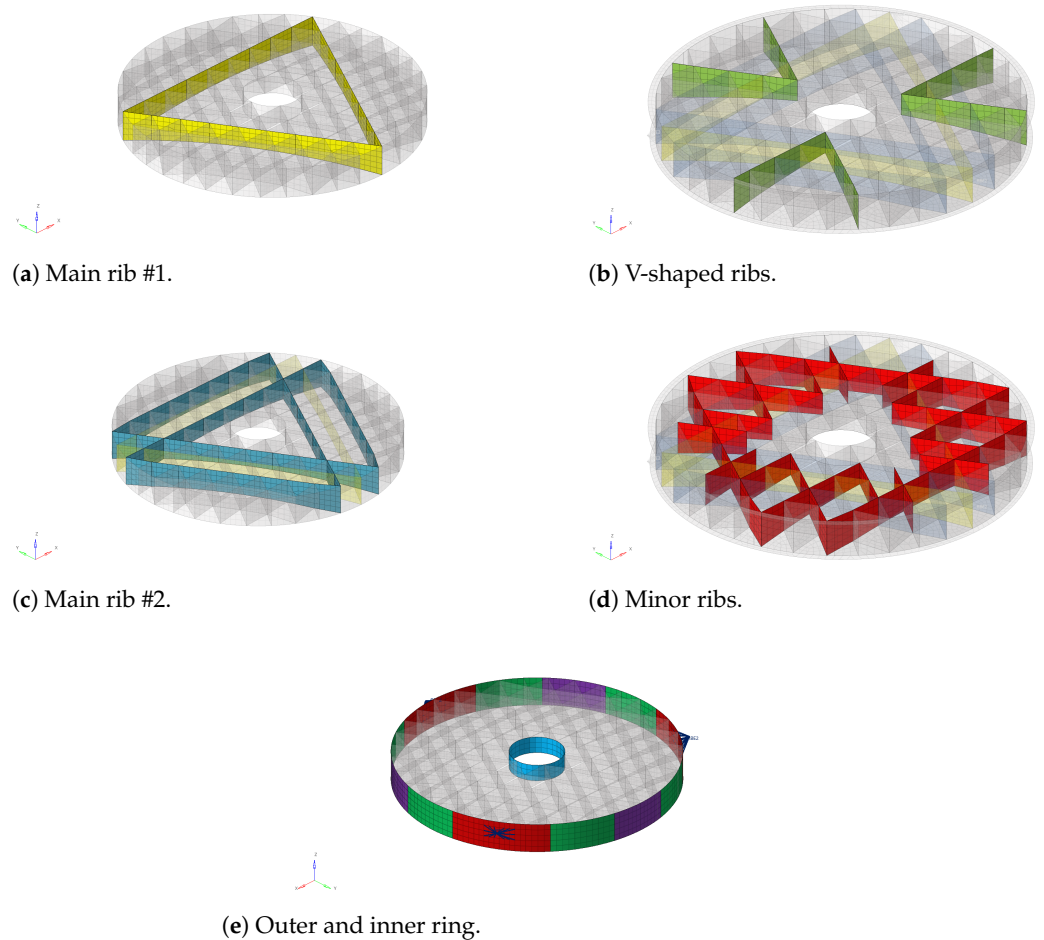
(**a**) Main rib #1.

(**b**) V-shaped ribs.

(**c**) Main rib #2.

(**d**) Minor ribs.

(**e**) Outer and inner ring.

Figure 4. Identified patterns contributing to overall performance.

2.5. Optimization Problem

In this sub-section, the mathematical optimization problem is described. Equation set (3) depicts the optimization problem being solved by *OptiStruct* using gradient-based algorithms. For this reason, all optimization responses have to be continuous and chosen such that non-convexity in terms of local optima is circumvented to the greatest extent possible. For more information on the challenging demands for gradient-based optimization, please refer to E. Wehrle [11].

$$\min_{\mathbf{x} \in \mathcal{X}} \{ \quad f(x) \quad | \quad g_j \leq 0 \} \tag{3}$$

Here, the objective function f shall be minimized by varying each design variable x_i (size and shape) within its bounds as described by the feasible design space $\mathcal{X}$. In Section 2.1, the assumptions made for breaking down WFE to the expression (4) are explained. Please note that this approach does not introduce any error or inaccuracy during optimization, but instead introduces a tremendous speed-up, in contrast to Zernike polynomials (see Equation (4)). Of course, Zernike polynomials were used to evaluate the optical performance of any of the derived optima. Equation (4) was therefore solely used for defining the search direction.

$$f(\mathbf{x}) = RMS(u^k_{z,rel}(x_i)) = \sqrt{\frac{1}{n} \sum_{k=1}^{n} u^k_{z,rel}{}^2} \tag{4}$$

In equation set (3), the inequality constraints g_j are defined as well. Fulfilling mass requirements is of importance in space telescope design, so they are mentioned at first

by inequality constraint g_1. Another relevant requirement is given by g_2, where the first—and therefore smallest—structural eigenfrequency ω shall be greater than the required minimum ω_{min}. Interestingly, ω increases in most of the conducted optimization and does not play a design-driving role in our investigated cases. For this reason, g_2 was not active and, in some cases, not considered during optimization runs, but it was checked at each found optima.

$$g_1 = m(x)/m_{max} - 1 \leq 0$$
$$g_2 = 1 - \omega(x)/\omega_{min} \leq 0$$

2.6. Investigated Load Cases

The research work focused on how the support case (either Figure 2a or Figure 2b of Figure 2) influences the optimal design of space mirrors. In order to do so, gravity release was realized for each scenario in the in-plane and out-of-plane direction, where the latter refers to a normal vector on the mirror's surface.

3. Baseline Performance

For the sake of comparison, a proper baseline is set up. This baseline is derived by experienced engineers. Thicknesses and contour have been chosen in one shot based on gained insights from former projects. Evidently, further design iterations would certainly improve the following results. However, they would necessitate the involvement of a design, as well as at least one analysis engineer. This process, where both disciplines would iteratively elaborate design improvements, may be regarded as cumbersome and demanding.

In Figures 5 and 6, the responses in terms of deformation and Zernike polynomials for derived baseline configuration are given for in-plane and out-of-plane loading, respectively. It shall be noted that these figures address the support configuration with outside support (see Figure 2a).
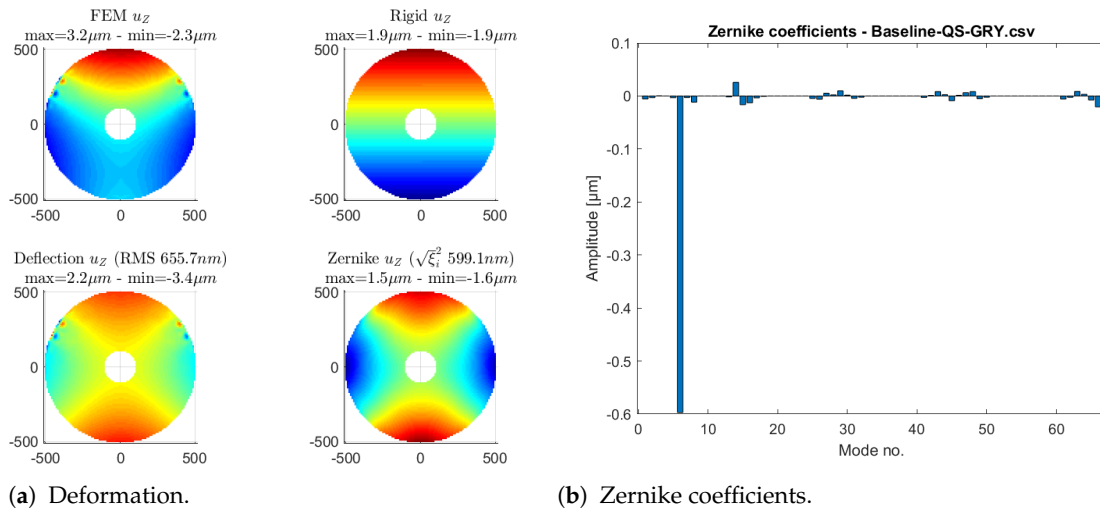

(**a**) Deformation.　　　　　　　　　　　　　(**b**) Zernike coefficients.

Figure 5. Baseline design with in-plane loading and outside support.

(**a**) Deformation.
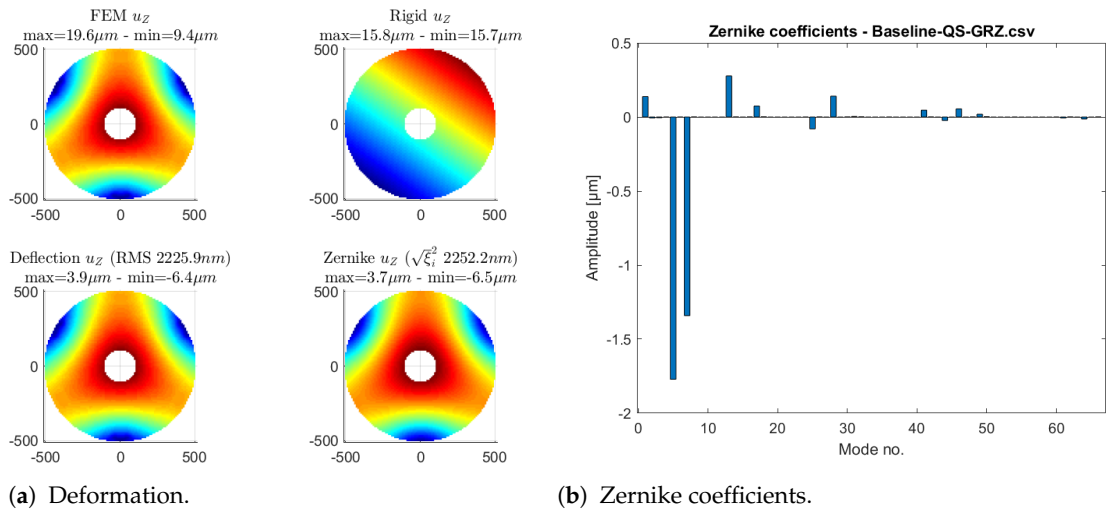
(**b**) Zernike coefficients.

Figure 6. Baseline design with out-of-plane loading and outside support.

It is worth mentioning that the upper right plot labeled *Rigid* (see Figures 5a and 8a) does not refer to mechanical rigid mode displacements but rather to potential rigid correction modes. These modes are determined by an *AIRBUS* internal tool and are relevant for the optical engineers to judge the severity of the mirror's surface deflection. This holds because a translation or tilt of the whole mirror (rigid) is realized with ease and shall therefore not be considered in the determination of wavefront errors or the like. Additionally, in rotational symmetry (see for instance Figures 8a and 11), there exists more than only one optimal rigid correction mode, which is why these may be regarded as local optima of equivalent rank.

Analogously to before, Figures 7 and 8 provide deformation and Zernike polynomials for baseline configuration for in-plane and out-of-plane loading. However, the two figures now correlate to the configuration with an inside support (see Figure 2b).
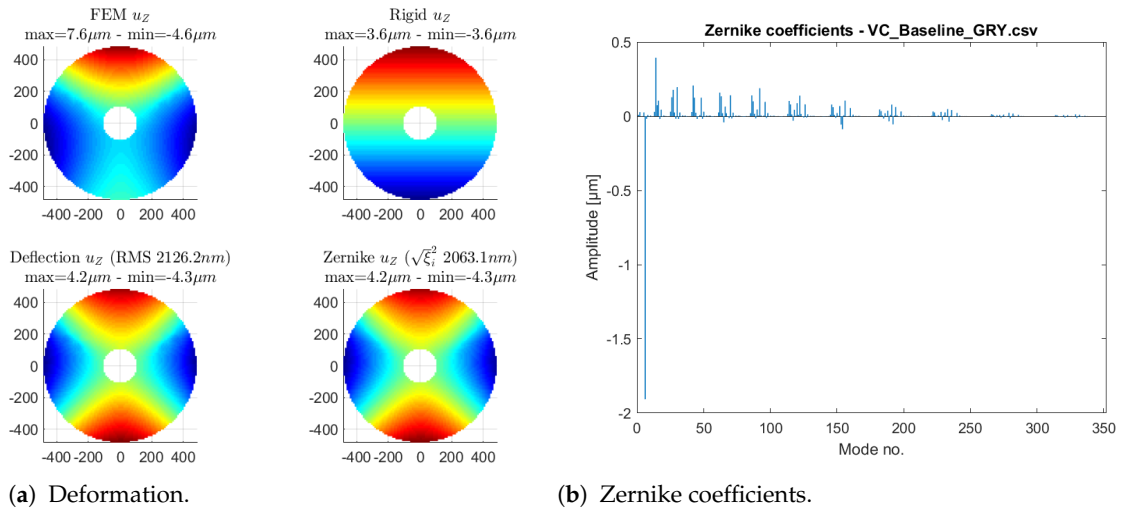

(**a**) Deformation.

(**b**) Zernike coefficients.

Figure 7. Baseline design with in-plane loading and inside support.

(a) Deformation.
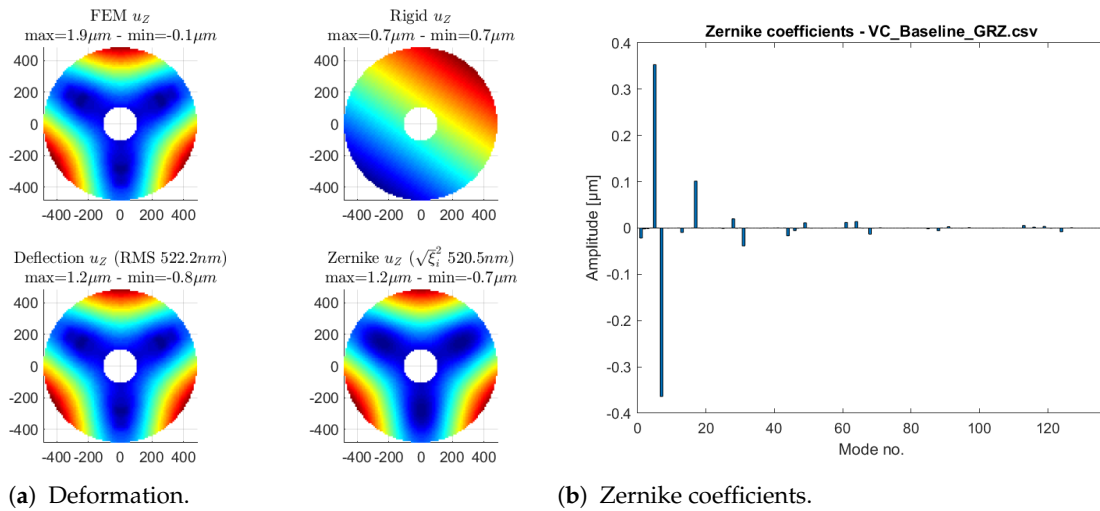

(b) Zernike coefficients.

Figure 8. Baseline design with out-of-plane loading and inside support.

4. Optimization Results

Within this section, optimization results are first given in tabular form, to provide a certain overview, and will be discussed afterwards.

4.1. Overview on Optima

In Table 1, an overview of all found optima is given. They are grouped by support case, as described in Section 2.2, where outer support refers to Figure 2a and inner support refers to Figure 2b. Furthermore, the results are categorized by the applied load case (LC). A distinction is made between in-plane loading (IP) and out-of-plane loading (OOP), and also which load case the mirror was optimized for. Responses are given by the root mean square of the deflections (RMS), where the improvement towards baseline design is referenced in percent by Δ. Sensitivity δ is also given for each optimization. Computation and interpretation of sensitivity δ is provided next, in Section 4.2.

Table 1. Overview of all found optima grouped over load case (LC) and support.

Support	Baseline		Optimized In-Plane				Optimized Out-Of-Plane			
	LC	RMS	LC	RMS	Δ	δ	LC	RMS	Δ	δ
outer	IP	655	IP	15	98%	5%	IP	130	80 %	7%
	OOP	2225	OOP	550	75%		OOP	370	85%	
inner	IP	2125	IP	120	94%		IP	700	67%	
	OOP	520	OOP	225	57%	0.7%	OOP	100	81%	2.4%

One may observe that in the case of outer supports, the RMS can be reduced best, when in-plane gravity release is foreseen. In the case of inner supports, out-of-plane gravity release actually provides slightly better results (RMS of 100 nm in contrast to 120 nm). Nonetheless, it may be concluded that a support configuration on the outer side of the mirror can be regarded as superior regarding the surface stability.

4.2. Robustness Evaluation

Next, the evaluation of robustness is discussed. This evaluation shall be based on already available sensitivities. These sensitivities were available as gradient-based optimization was deployed. For this reason, the following robustness evaluation ought to be realized after each optimization run as part of a thorough post-processing.

Imagine a linear system, with x being the variable, a and b the mathematical constants, and, last but not least, y a linear response, as given by Equation (5).

$$y = ax + b \tag{5}$$

Note that $\overline{X}$ represents the mean and σ_x the standard deviation of x in the following. These statistical quantities may be computed for linear systems—such as the one of Equation (5)—via Equation (6) [12].

$$\overline{Y} = a\overline{X} + b$$
$$\sigma_y^2 = b\sigma_x^2 \tag{6}$$

Knowing this, the overall optimization response on $RMS(u_{z,rel}^k(x_i))$ (see Equation (4)) is to be judged based on the variation of each design variable x_i via the standard deviation σ_{x_i}. This is realized by the following Equation (7), where a linearization at the optimum is performed.

$$\sigma_{RMS}^2 = \sigma_f^2 = \sum_{i=1}^{n_{DV}} \frac{\partial f}{\partial x_i} \sigma_{x_i}^2 \tag{7}$$

This approach has been used to evaluate each optimum's robustness, as depicted in Table 1. In some cases, the linearization evidently introduces a slight error; however, the outlined approach does still allows a comparison of different optima and therefore yields an increase in overall robustness. This is the case because smaller indicated sensitivity values point to directions for design improvement. For more information on this topic, the reader is directed to S.A. Uebelhart and his dissertation [13].

4.3. Convergence Behavior

In the following plots of Figure 9, a representative convergence plot is given. As illustrated, the optimization converges rather fast at the beginning—within the first five iterations—and then slows down, starting from the tenth iteration. The improvements are, however, still relevant. This might be comprehended by studying Figure 9b, as a further reduction is to be observed when using a semi-logarithmic scale.
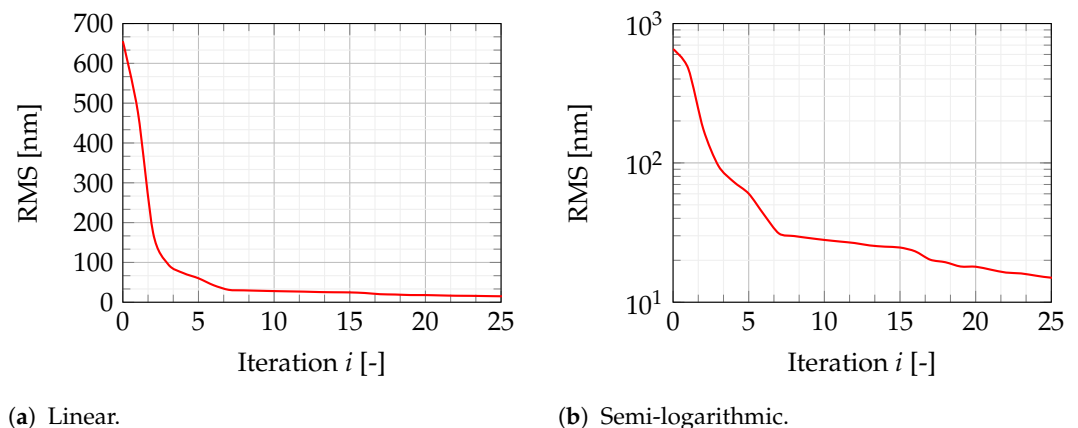

(**a**) Linear.   (**b**) Semi-logarithmic.

Figure 9. Convergence plots of OOP optimization inner support case.

Here, it shall be highlighted that *OptiStruct* is based on gradient-based optimization, which allows an efficient convergence. Alternatively, a generic algorithm has been tried as well; however, the multitude of variables (and the resulting curse of dimensionality) did not allow for relevant design improvements. This particularly holds in the case of the optimum of interest, which is feasible from a technical perspective.

4.4. Optimization Results and Figures

In Section 4.1, an overview of all optima is provided. Figure 10 depicts the deformation and Zernike polynomials of the optimization case: the minimization of in-plane responses (IP). The support for this optimization case was realized outside, as depicted in Figure 2a.
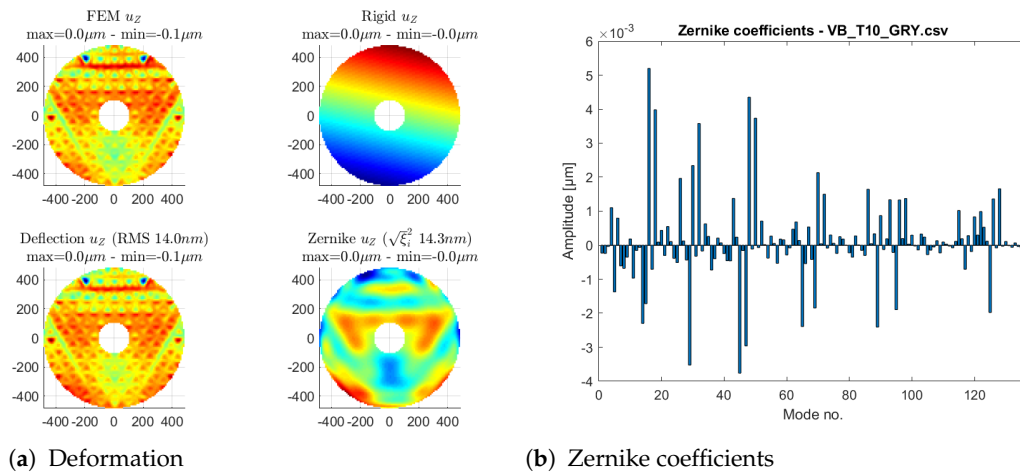

(**a**) Deformation   (**b**) Zernike coefficients

Figure 10. Optimum (optimization conducted on IP responses) and outside support.

The following Figure 11 depicts the deformation and Zernike polynomials of the minimization of the out-of-plane responses (OOP) optimization case. The support for this optimization case was realized inside, as depicted in Figure 2b.
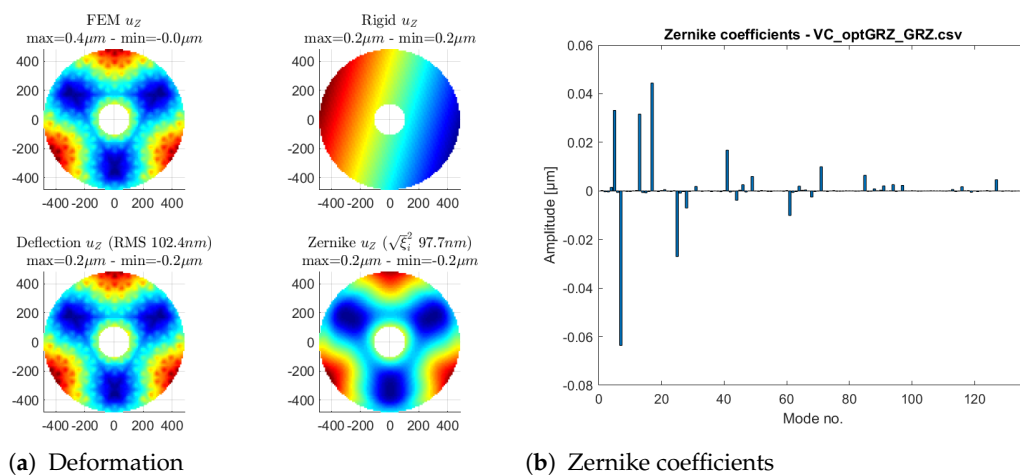

(**a**) Deformation   (**b**) Zernike coefficients

Figure 11. Optimum (optimization conducted on OP responses) and inside support.

4.5. Design Variable Changes

In this section, the change in design variables shall be discussed. The goal is to increase transparency and allow the reader to comprehend our findings, by taking a look at the design space and contrasting the initial values to those at the optimum. At this point, it is relevant to note that the optimum may be assumed to be global, as multiple optimization with different starting points yielded the same design variable vector. However, as we do not have a solid proof for a convexity, the displayed optimum has to be regarded as local.

In Table 2, the above-mentioned design space is given. Note that the found design variable vector x_{opt} is feasible, as it lies within the defined bounds (i.e., lower design variable bound x_l and upper x_u, respectively). By further studying this, one may observe that some of the values are right at the bounds and are therefore highlighted in red. There are basically two categories. First, there are the ones that are sizing variables. Some of the rib groups, for instance minor ribs, tend to the lower bound of 0.5. This bound has been set because manufacturing dictated a minimum of 0.5 mm. The second category is formed

by shape variables. These variables tend to the greatest value (i.e., upper bound). These bounds have been set because the mirror shall remain within its physical design space, and therefore it cannot violate, for instance, its maximum allowable height.

Table 2. Design variables at starting point x_0 and at found "local" optimum x_{opt} with their corresponding bounds (lower x_l and upper x_u).

ID	Label	Type	x_l	x_u	x_0	x_{opt}
1	T-ORing	size	0.5	4.0	2.0	0.693
2	T-Minor	size	0.5	4.0	1.5	0.500
3	T-Mirror	size	0.5	4.0	2.0	1.222
8	T-MR1	size	0.5	4.0	2.0	1.533
9	T-MR2	size	0.5	4.0	2.0	3.988
10	S-MR1-1	shape	−0.5	1.0	0.0	−0.081
11	S-MR1-2	shape	−0.5	1.0	0.0	1.000
13	S-MR2-2	shape	−0.5	1.0	0.0	0.325
14	S-MR2-3	shape	−0.5	1.0	0.0	0.160
15	S-MR2-4	shape	−0.5	1.0	0.0	1.000
17	S-MR2-5	shape	−0.5	1.0	0.0	1.000
18	T2-MR1	size	0.5	4.0	1.0	1.318
20	T3-MR2	size	0.5	4.0	1.0	1.229
21	T4-MR2	size	0.5	4.0	1.0	1.749
22	T-IRing	size	0.5	4.0	3.0	2.135
23	T-ORingC	size	0.5	4.0	3.0	0.500
24	T-ORingA	size	0.5	8.0	3.0	6.059
25	T-cent	size	0.5	4.0	2.0	0.529
28	T2-MR2	size	0.5	4.0	2.0	2.538
29	T-ears	size	0.5	4.0	2.0	0.572
30	S-Ring	shape	−0.5	1.0	0.0	1.000
32	T-CProf	size	0.5	4.0	2.0	0.699
33	T-OutRib	size	0.5	4.0	2.0	0.594
34	T-cross	size	0.5	4.0	2.0	3.898
38	Bl-Long	shape	−0.5	1.0	0.0	0.008
39	Bl-short	shape	−0.5	1.0	0.0	1.000
40	T-V	size	0.5	4.0	2.0	1.491
41	V1	shape	−0.5	1.0	0.0	−0.002
42	V2	shape	−0.5	1.0	0.0	−0.002
43	Minor	shape	−0.5	1.0	0.0	−0.002

Of course, the reader may write to the authors in order to obtain all further details required in order to study the results in even greater depth.

5. Conclusions

In Section 4.1, an overview of all found optima was given. By studying Table 1 within this section, it is revealed that inner support of the mirror structures is particularly beneficial in the case where in-plane (IP) gravity removal is realizable. From a technical perspective, this is advantageous, as in-plane gravity release is a manufacturing and, even more relevantly, an optical verification measurement, where earth's gravity load would lie in-plane (IP) of the mirror. Hence, the mirror could be placed standing perpendicular with respect to the ground. This would then also mean that the measuring distance does not necessitate huge buildings, simplifying the optical ground support equipment and lowering costs compared to out-of-plane measurement.

In contrast, the inner support is performs slightly better when optimization is performed on responses in the out-of-plane (OOP) direction. However, the difference between a support on the inner side towards the outer side of the mirror is actually rather slight.

Optimization, in general, yields drastic optical performance increases. However, it also brings forth local deformations under gravity removal, which in turn translate to higher Zernike polynomials. These higher polynomials are, in many cases, challenging in terms of overall telescope design. This is why lower-order polynomials are generally desired. Nonetheless, one might use underlying minor rib structures to prevent higher-order Zernike polynomials from occurring by accepting slight reductions in overall optical performance (i.e., a higher wavefront error (WFE)). In general, therefore, one might state that for local ribs (see, for instance, Figure 4c), a slight deviation from the optimal thickness may increase the WFE but, at the same time, reduce the order of Zernike polynomials, thus offering the possibility of compensating the lower-order Zernike modes via active optics.

Studying the robustness of all derived optima revealed that, in general, the sensitivity can be regarded as low towards design variable changes. This actually means that imperfections experienced during manufacturing or similar inaccuracies do not depreciate optical performance. It shall also be highlighted that robustness is evaluated with ease, as the necessary sensitivities are already available from the optimization that was conducted based on gradient-based algorithms.

In conducting our studies, we did find that optimizing for optical performance generally yields lighter mirror structures as well. Hence, there is generally no conflict between the objectives minimum surface error and minimum weight. This becomes evident in considering gravitational loads. However, as highlighted before, once local deformation modes (as displayed in Figure 10) are to be mitigated, slight increases in mass have be considered.

Regarding tooling and software, the use of *Altair*'s FEM software clearly supported the conducted research work. The use of *HyperMesh*, in tandem with *OptiStruct*, allowed the introduction of a great degree of freedom in design. It was an ease to create perturbation functions (morphing) for individual ribs, while still honoring the mechanical link between all other structural elements. By doing so, their height contour variations were independent and free to change within the optimization. However, each rib was tied to all surrounding ones, as they are linked via special contact definitions. These definitions were updated by each iteration of the optimization, allowing a smooth and robust shape optimization. This technique allows great flexibility in placing ribs in the initial design, allowing the possibility of studying a great multitude of cases.

6. Outlook

Next, vector optimization with two objectives will be perfomed. One objective clearly remains the increase of overall optical performance. The additional objective will be the order of Zernike polynomials. This shall provide more insight into how minor ribs help to balance the negative side effects of strongly optimized mirrors, which are prone to high-order Zernike polynomials.

Author Contributions: Conceptualization, S.L. (Airbus telescope expert) and M.E.S.; methodology, M.W., M.E.S., and C.J.; software, M.W. and C.J.; formal analysis and structural optimization, M.W., M.E.S., and C.J.; investigation, M.W.; writing, all equally; project administration, S.L.; funding acquisition, C.J. All authors have read and agreed to the published version of the manuscript.

Institutional Review Board Statement: Not applicable.

Data Availability Statement: All generated results are accessible upon request.

Conflicts of Interest: The authors declare no conflict of interest.

Abbreviations

Overview on the used symbols.

Abbreviation	Definition	Unit
$\vec{u}^i$	Displacement of node i	m
$\bar{\bar{u}}$	Displacement of rigid surface at center	m
$\bar{\bar{\theta}}$	Tilt of rigid surface at center	rad
$\vec{r}^i$	Geometric lever of node i towards center	m
$\vec{u}^i_{rel}$	Relative displacement of node i	m
$f(x)$	Objective function	1
$g(x)$	Inequality constraint function	1
x	Design variable	1
$\mathcal{X}$	Feasible design space	1
m	Mass	kg
$\rightarrow$	Eigenfrequency	s^{-1}
ξ_i	Coefficients of Zernike polynomials	1

References

1. Nigdeli, S.M.; Bekdaş, G.; Kayabekir, A.E.; Yucel, M. *Advances in Structural Engineering—Optimization-Emerging Trends in Structural Optimization*; Springer Nature: Singapore, 2020.
2. Eberle, S. Minimierung von Verformungsfehlern Eines Rippenversteiften, Optischen Spiegels mit Piezoaktoren und Faseroptischer Sensorik. Master's Thesis, Technische Universität München, München, Germany, 2006.
3. Müller, U. Structural Monitoring and Displacement Field Estimation Based on Distributed Fiber Bragg Grating Sensors. Dissertation, Technical University of Munich, Munich, Germany, 2009.
4. Liu, S.; Rui, H.; Li, Q.; Zhou, P.; Dong, Z.; Kang, R. Topology optimization-based lightweight primary mirror design of a large-aperture space telescope. *Appl. Opt.* **2014**, *53*, 8318–8325. [CrossRef] [PubMed]
5. Lucarelli, S.; Brandt, N. Interdisciplinary optimisation of the structural spacecraft interface for the LISA technology package. *Spacecr. Struct. Mater. Mech. Test.* **2005**, *581*, 30.
6. Qu, Y.; Jiang, Y.; Feng, L.; Li, X.; Liu, B.; Wang, W. Lightweight Design of Multi-Objective Topology for a Large-Aperture Space Mirror. *Appl. Sci.* **2018**, *8*, 2259. doi: 10.3390/app8112259. [CrossRef]
7. Sigmund, O.; Aage, N.; Andreassen, E. On the (non-)optimality of Michell structures. *Struct. Multidiscip. Optim.* **2016**, *54*, 361–373. [CrossRef]
8. Schatz, M.E.; Hermanutz, A.; Baier, H.J. Multi-criteria optimization of an aircraft propeller considering manufacturing. *Struct. Multidiscip. Optim.* **2017**, *55*, 899–911. doi: 10.1007/s00158-016-1541-z. [CrossRef]
9. Zernike, v.F. Beugungstheorie des schneidenver-fahrens und seiner verbesserten form, der phasenkontrastmethode. *Physica* **1934**, *1*, 689–704. doi: 10.1016/S0031-8914(34)80259-5. [CrossRef]
10. Bely, P.Y. *The Design and Construction of Large Optical Telescopes*; Springer: New York, NY, USA, 2003.
11. Wehrle, E.; Gufler, V. Lightweight Engineering Design of Nonlinear Dynamic Systems with Gradient-Based Structural Design Optimization; Springer: Berlin/Heidelberg, Germany, 2021; pp. 44–57. doi: 10.1007/978-3-662-63143-0_5. [CrossRef]
12. Jaynes, E.T. *Probability Theory: The Logic of Science*; Cambridge University Press: Cambridge, UK, 2003. doi: 10.1017/CBO9780511790423. [CrossRef]
13. Uebelhart, S.A. Non-Deterministic Design and Analysis of Parameterized Optical Structures during Conceptual Design. Dissertation, Massachusetts Institute of Technology, Cambridge, MA, USA, 2006.